Title

Conformational Dynamics in the Interaction of SARS-CoV-2 Papain-like Protease with Human Interferon-Stimulated Gene 15 Protein

Journal

The Journal of Physical Chemistry Letters, 12(23)

ISSN

1948-7185

Authors

Leite, Wellington C

Weiss, Kevin L

Phillips, Gwyndalyn

et al.

Publication Date

2021-06-17

DOI

10.1021/acs.jpclett.1c00831

Peer reviewed

THE JOURNAL OF PHYSICAL CHEMISTRY LETTERS
A JOURNAL OF THE AMERICAN CHEMICAL SOCIETY

pubs.acs.org/JPCL

Letter

Conformational Dynamics in the Interaction of SARS-CoV-2 Papain-like Protease with Human Interferon-Stimulated Gene 15 Protein

Wellington C. Leite, Kevin L. Weiss, Gwyndalyn Phillips, Qiu Zhang, Shuo Qian, Susan E. Tsutakawa, Leighton Coates,* and Hugh O'Neill*

Cite This: *J. Phys. Chem. Lett.* 2021, 12, 5608–5615

Read Online

ACCESS | Metrics & More | Article Recommendations | Supporting Information

ABSTRACT: Papain-like protease (PLpro) from SARS-CoV-2 plays essential roles in the replication cycle of the virus. In particular, it preferentially interacts with and cleaves human interferon-stimulated gene 15 (hISG15) to suppress the innate immune response of the host. We used small-angle X-ray and neutron scattering combined with computational techniques to study the mechanism of interaction of SARS-CoV-2 PLpro with hISG15. We showed that hISG15 undergoes a transition from an extended to a compact state after binding to PLpro, a conformation that has not been previously observed in complexes of SARS-CoV-2 PLpro with ISG15 from other species. Furthermore, computational analysis showed significant conformational flexibility in the ISG15 N-terminal domain, suggesting that it is weakly bound to PLpro and supports a binding mechanism that is dominated by the C-terminal ISG15 domain. This study fundamentally improves our understanding of the SARS-CoV-2 deISGylation complex that will help guide development of COVID-19 therapeutics targeting this complex.

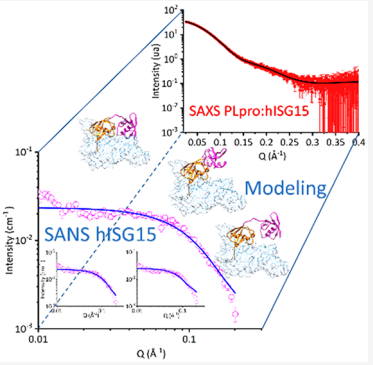

Severe acute respiratory syndrome coronavirus 2 (SARS-CoV-2) is currently causing a worldwide pandemic,[1] underscoring the need for an improved understanding of its replication machinery. Like earlier coronaviruses, MERS-CoV and SARS-CoV, this virus utilizes two cysteine proteases [the main protease,[2,3] also called nonstructural protein 5, and papain-like protease (PLpro), which is a small domain of the larger nonstructural protein 3 (Nsp3)][4] to generate a functional replicase complex that is required for the virus to spread. SARS-CoV PLpro cleaves the viral polyprotein pp1a at three sites at the N-terminus (177LNGG ↓ AVT183, 815LKGG ↓ API821, and 2737LKGG ↓ KIV2743) to release mature Nsp1, Nsp2, and Nsp3, respectively.[5] PLpro also removes interferon-stimulated gene 15 protein (ISG15) and ubiquitin from host proteins to negatively impact the innate immune response. In animals, the amino acid sequences of ISG15 exhibit significant diversity, with the amino acid sequence identity ranging from 65.8% to 34.5% from human to mouse, and human to insect, ISG15, respectively.[6] The addition of ubiquitin to lysine side chains is a common post-translational modification that regulates protein activity, often via targeted degradation. ISG15 is also conjugated to target proteins in a process called ISGylation, a regulatory process that targets the protein for proteasomal degradation.[7] ISGylation and ubiquitination both play vital roles in the regulation of the immune response to viral infection. Thus, many viruses have developed strategies for disrupting these pathways.

Recent biochemical and structural studies[8,9] have compared the activities of PLpro from SARS-CoV and SARS-CoV-2. While they have a sequence identity of 83%, these studies showed that the deISGylating and deubiquitylating activities of PLpro from SARS-CoV and SARS-CoV-2 differ in their substrate preference. PLpro from SARS-CoV-2 was shown to be more efficient at cleaving ISG15 than ubiquitin molecules, the opposite of the result for PLpro from SARS-CoV.[8,9] Not unexpectedly, crystal structures of the mouse ISGS15 PLpro complex revealed that the mode of binding of ISG15 by SARS-CoV-2 PLpro and SARS-CoV PLpro was conserved.[8] Mutation studies in the S2 helix binding site of the PLpro from SARS-CoV-2 indicated that upon introduction of a hydrophobic residue at position 76, the deubiquitylating activity of PLpro from SARS-CoV-2 was increased compared to that of the wild-type enzyme. However, to date, there has been a lack of structural information regarding SARS-CoV-2 PLpro in complex with the full length, more clinically relevant human ISG15,[10] which shares 65.8% amino acid sequence identity with mouse ISG15.[6] Human ISG15 is composed of two ubiquitin-like domains connected by a flexible linker, suggesting that the two domains may be able to move freely and independently of each other.[10] Earlier studies of PLpro from SARS-CoV have shown that it contains two ubiquitin-like

Received: March 14, 2021
Accepted: May 18, 2021
Published: June 10, 2021

https://doi.org/10.1021/acs.jpclett.1c00831
J. Phys. Chem. Lett. 2021, 12, 5608–5615

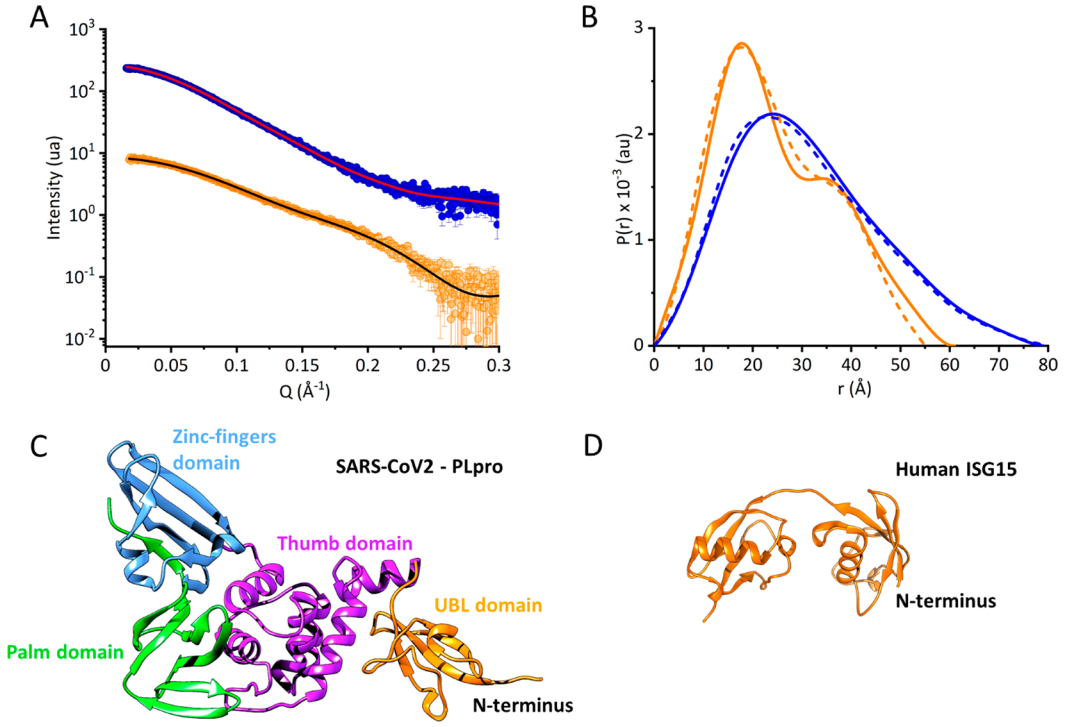

Figure 1. SAXS analysis of SARS-CoV-2 PLpro C111S and human ISG15 in solution. (A and B) SAXS and $P(r)$ profiles for PLpro C111S (blue) and hISG15 (orange), respectively. The theoretical $P(r)$ profiles of free hISG15 and PLpro C111S are shown as dashed lines using the same color scheme as the experimental data. The SAXS curves are offset by a factor of 10 for the sake of clarity. The fit curves for the theoretical SAXS curves calculated from the respective crystal structures are overlaid on SAXS curves as solid red and black lines. (C) PLpro C111S crystal structure (PDB entry 7D6H) with the palm, thumb, zinc-finger, and ubiquitin-like (UBL) domains highlighted. (D) Crystal structure of hISG15 (PDB entry 1Z2M).

Table 1. SAS Structural Parameters and Data Fitting

	PLpro C111S alone	PLpro C111S alone	PLpro C111S in complex	hISG15 alone	hISG15 alone	hISG15 in complex	PLpro C111:hISG15 complex
SAS technique employed	SEC-SAXS	SANS	SANS	SEC-SAXS	SANS	SANS	SEC-SAXS
protein concentration (mg mL^{-1})	varies	5.0	6.2	varies	3.1	2.9	varies
Guinier analysis							
$I(0)$ (cm^{-1})	25.52 ± 0.04	0.22 ± 0.01	0.26 ± 0.01	8.68 ± 0.03	0.04 ± 0.01	0.02 ± 0.01	38.40 ± 0.08
R_g (Å)	23.7 ± 0.1	24.0 ± 0.1	24.5 ± 0.1	19.3 ± 0.1	17.4 ± 0.6	15.5 ± 0.5	24.9 ± 0.1
QR_g range	0.49−1.29	0.22−1.23	0.26−1.23	0.34−1.28	0.12−1.30	0.48−1.26	0.65−1.29
$P(r)$ analysis							
$I(0)$ (cm^{-1})	25.7 ± 0.1[a]	0.22 ± 0.01	0.25 ± 0.01	8.74 ± 0.03[a]	0.04 ± 0.03	0.02 ± 0.01	38.6 ± 0.1[a]
R_g (Å)	24.3 ± 0.1	24.5 ± 0.2	24.7 ± 0.1	19.3 ± 0.1	18.6 ± 0.5	15.1 ± 0.3	25.2 ± 0.1
D_{max} (Å)	80	80	78	62	60	44	79
Q range (Å^{-1})	0.02−0.3	0.01−0.25	0.009−0.20	0.018−0.40	0.015−0.30	0.012−0.20	0.02−0.3
χ^2	1.6	3.9	1.8	<1	<1	1.5	1.9
molecular weight (M_W) analysis							
M_W from Porod volume (kDa)	34.7	34.7	39.1	16.2	16.4	16.8	49.0

[a] $I(0)$ from SEC-SAXS is not on an absolute scale. Theoretical molecular masses of PLpro C111S and hISG15 are 36.0 and 17.0 kDa, respectively.

domains that engage with the N-terminus of ISG15s.[6] Human and mouse ISG15s possess similar secondary structures in the two ubiquitin-like domains, but significant differences are present in the tertiary structures of mouse ISG15 and human ISG15 (Figure S1). Several studies have focused on developing inhibitors that target the groove-like pocket of PLpro that binds the C-terminus of human and mouse ISG15s.[8,11] *In silico* and *in vitro* studies identified molecules such as VIR250 and VIR251,[12] GRL-0617,[8,13] and rac5c[11,14] that may be good candidates for preventing PLpro deISGylation activity by binding in this pocket to prevent binding of ISG15.

To aid in our understanding of human ISG15 recognition by SARS-CoV-2 PLpro, small-angle X-ray and small-angle neutron scattering (SAXS and SANS, respectively) were used to investigate their interaction in solution. These measurements have allowed us to study the conformation of SARS-CoV-2 PLpro and hISG15 independently and in complex with each other to provide new insights into the relative orientation

https://doi.org/10.1021/acs.jpclett.1c00831
J. Phys. Chem. Lett. 2021, 12, 5608−5615

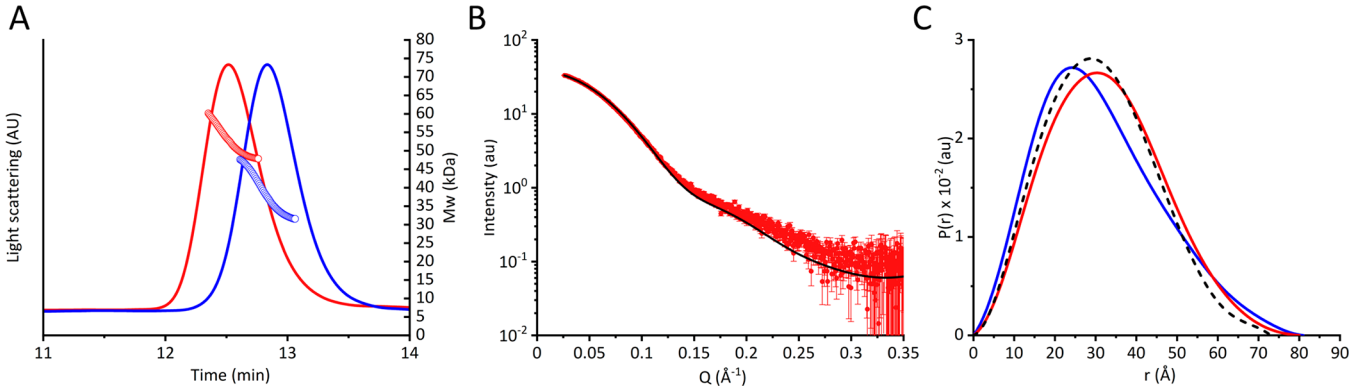

Figure 2. Combined size exclusion chromatography and small-angle X-ray scattering analysis of the PLpro C111S:hISG15 complex. (A) SEC-MALS elution profile of PLpro C111S and the PLpro C111S:hISG15 complex, shown with blue and red lines, respectively. (B) Experimental SAXS profile of the PLpro C111S:hISG15 complex and theoretical SAXS curve for the PLpro:mISG15 complex (PDB entry 6YVA), shown as red circles and black lines, respectively. (C) $P(r)$ function of PLpro C111S alone (blue line) and PLpro C111S in complex with hISG15 (red line) and theoretical $P(r)$ function for the PLpro mISG15 complex (black dashed line).

of the proteins in the complex. We used the catalytically inactive variant PLpro C111S (termed PLpro henceforth) to allow the intact complex to be studied without unwanted proteolysis reactions for all measurements. The protiated and partially deuterated proteins were overexpressed and purified from *Escherichia coli* cultures as described in the Supporting Information. The mature form of hISG15 was obtained commercially (Bio-Techne, Minneapolis, MN, catalog no. UL-601). SAXS coupled with multiangle light scattering and size exclusion chromatography (SEC-SAXS-MALS) experiments were performed at Advanced Light Source beamline 12.3.1 at Lawrence Berkley National Laboratory.[15,16] SANS studies were performed using the Bio-SANS instrument located at the High Flux Isotope Reactor at Oak Ridge National Laboratory.[17,18] A detailed description of the data analysis approaches used is provided in the Supporting Information. SEC-SAXS yielded a radius of gyration (R_g) and a maximum dimension (D_{max}) of 23.6 ± 0.1 and 80 Å, respectively (Figure 1A and Table 1). The molecular mass calculated from SAXS (34 kDa) was within the accuracy range calculated from the amino acid sequence (36.0 kDa), indicating that the protein exists as a monomer in solution. The pair distance distribution function [$P(r)$] curve of free PLpro supports the idea that it is in an extended conformation (Figure 1B). SANS data agree with SAXS data, yielding similar structural parameters [R_g and D_{max} of 24.1 ± 0.1 and 80 Å, respectively (see Figure S2A and Table 1)]. The PLpro C111S crystal structure [Protein Data Bank (PDB) entry 7D6H] shows good agreement with the SAXS and SANS data (χ^2 = 1.9 and 2.8, respectively), indicating that the catalytic ubiquitin-specific protease (USP) and ubiquitin-like domains are in a similar conformation in solution as the crystal structures (Figure 1A and Figure S2A). The USP encompasses thumb, palm, and zinc-finger subdomains (Figure 1C).[19] However, closer examination of the theoretical (PDB entry 7D6H) and experimental PLpro C111S $P(r)$ curves shows a slight shift in the peak position from 22 to 25 Å, suggesting differences in the crystal and solution structures of the protein (Figure 1B). It was previously shown that the ubiquitin-like domain of SARS-CoV-1 PLpro can adopt at least two different conformations that could explain the differences in the $P(r)$ profiles observed here.[6]

ISG15 is an interferon-α/β-induced, ubiquitin-like protein that is conjugated to a wide array of cellular proteins. The hISG15 structure has the N- and C-terminal ubiquitin-like domains, each of which assumes a β-grasp fold structure that is nearly identical to that found in ubiquitin (Figure 1D).[10] SAXS analysis of hISG15 yielded an R_g and a D_{max} of 19.2 ± 0.1 and 62 Å, respectively (Table 1). The SAXS-derived molecular mass was 16.2 kDa, indicating that it is a monomer in solution and consistent with the molecular mass calculated from the amino acid sequence (17.0 kDa). There was excellent agreement between the theoretical scattering curve of hISG15 derived from its crystal structure (PDB entry 1Z2M) and the experimental SAXS and SANS data (χ^2 = 1.6 and 0.9, respectively) (Figure 1A and Figure S2B), indicating a similar conformation of the protein in solution as observed in the crystal structure (PDB entry 1Z2M). The $P(r)$ analysis of hISG15 shows a bimodal distribution of interatomic distances between two well-separated ubiquitin-like domains in the experimental and theoretical (PDB entry 1Z2M) profiles (Figure 1B). However, the peak at ∼35 Å in the $P(r)$ profile is more prominent and shifted to longer distances compared to the theoretical profile, indicating that the two domains of hISG15 in solution are more separated than in the crystal structure. Langley et al.[20] compared human, mouse, and bat ISG15 structures (PDB entries 1Z2M, 5TLA, and 6MDH, respectively) and showed a difference in the twist around the N- and C-terminal domains that could be attributed to differences in the flexible hinge region connecting the two domains. Calculation of the theoretical $P(r)$ profiles of these proteins also presents the expected bimodal distribution. However, the position of the second peak (∼35 Å) is shifted among the curves supporting the crystallographic analysis (Figure S6). Interestingly, the $P(r)$ distributions of hISG15 from SAXS and bat ISG15 are most similar, providing additional evidence that the relative orientation of the domains in hISG15 is different in the crystal structure and in solution. This suggests a conformational flexibility in hISG15 in solution that may be important for protein−protein interactions.

Size exclusion chromatography (SEC) showed that PLpro and hISG15 form a 1:1 complex (Figure S3A). In addition, sodium dodecyl sulfate−polyacrylamide gel electrophoresis analysis confirmed that there is no proteolysis of either PLpro or ISG15 (Figure S3B). SEC-SAXS determined that the R_g and

https://doi.org/10.1021/acs.jpclett.1c00831
J. Phys. Chem. Lett. 2021, 12, 5608−5615

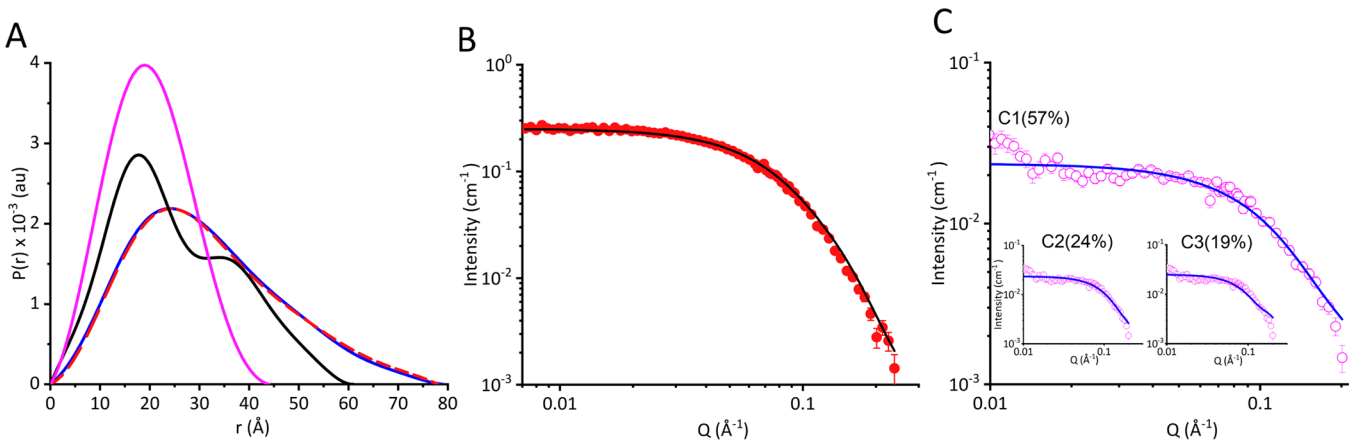

Figure 3. SANS analysis of the PLpro C111S:hISG15 complex. (A) $P(r)$ curves for free PLpro C111S (blue), deuterated PLpro C111S in the complex (red), free hISG15 in solution (black), and hISG15 in the complex (magenta). (B) Contrast-matched SANS profiles for bound PLpro C111S (red circles) in 42% D_2O. The fit curve calculated from the PLpro C111S crystal structure (PDB entry 7D6H) is shown as a black line. (C) Bound hISG15 (pink circles) in 100% D_2O. The theoretical SANS curves calculated for hISG15 conformers C1−C3 obtained from BILBOMD are shown as light blue lines. The insets show the fit of hISG15 conformers C2 and C3, while the main plot shows the fit of conformer C1.

D_{max} of the PLpro:hISG15 complex were 24.3 ± 0.4 and 79 Å, respectively (Figure 2A and Table 1). Interestingly, these values are remarkably similar to the structural parameters of PLpro alone (25.6 ± 0.1 and 80 Å, respectively). However, the shape of the $P(r)$ curve for the complex is more symmetrical, and the peak is shifted to longer distances, suggesting that the complex has a more globular shape compared to that of PLpro alone, which is more elongated (Figure 2C). Unexpectedly, the scattering curve predicted from the recently published crystal structure of the PLpro:mouse ISG15 (mISG15) complex (PDB entry 6YVA) does not fit the data well (χ^2 = 4.9), indicating differences in how PLpro interacts with hISG15 (Figure 2B).

To better understand the structural differences between the PLpro:mISG15 and PLpro:hISG15 complexes, we performed SANS with contrast matching to selectively highlight the individual components in the complex. Deuterated PLpro was prepared as described in the Supporting Information. SANS measurements were performed in 42% and 100% D_2O buffers to selectively highlight the scattering contribution of deuterated PLpro and protiated hISG15, respectively, while minimizing the scattering from its binding partner in the complex.

In the case of PLpro, the $P(r)$ profiles of the free and bound proteins are similar, indicating that its conformation remains largely unchanged when bound to hISG15 (Figure 3A). The small differences are more readily observed by representing the data as a normalized Kratky plot (Figure S4A). The profiles are similar over the measured Q range except for a slight deviation at larger scattering angles (0.09 Å^{-1} < Q < 0.24 Å^{-1}). The shape of the profile is typical for a well-folded protein showing a peak that decays with an increase in Q. The sharper decrease in the slope in the high-Q region for the bound protein indicates that PLpro has a more compact conformation than the free protein. A fit of free PLpro (PDB entry 7D6H) to the SANS data of the bound protein shows good agreement over the measured Q range. However, the fit deviates in the mid-Q region (~0.05 to 0.2 Å^{-1}), supporting differences in the arrangement of the individual domains between the free and bound protein (χ^2 = 6.7) (Figure 3B). Furthermore, a fit of the bound PLpro structure from the PLpro:mISG15 complex with the SANS data also deviates in the mid-Q range, suggesting that the PLpro in complex with hISG15 is different from when it is bound to mISG15 [χ^2 = 8.5 (Figure S5)].

Analysis of the hISG15 SANS data tells a very different story. As described above, the $P(r)$ profile of free hISG15 is bimodal, consistent with well-separated ubiquitin-like domains (Figure 1B). However, when hISG15 is bound to PLpro, the $P(r)$ profile undergoes a transition to a single symmetrical peak, and the D_{max} is decreased from ~62 to ~44 Å, indicating the overall conformation of ISG15 is now more compact (Figure 3A). In addition, SANS analysis of bound hISG15 yielded an R_g (15.5 ± 0.5 Å) that was much smaller than that of the free protein (19.2 ± 0.1 Å). Furthermore, Kratky analysis shows that the free hISG15 profile plateaus at a high Q, which is characteristic of a flexible, dynamic protein.[21] In contrast, the bound protein has a well-defined bell-shaped profile of a compact globular protein (Figure S4B).[22] The theoretical $P(r)$ profile of mISG15 bound to PLpro (PDB entry 6YVA) retains its bimodal shape observed for its unbound counterpart. It has a longer D_{max} (~55 Å) compared to that of bound hISG15 (~44 Å), demonstrating that the interactions of mISG15 and hISG15 with PLpro are significantly different (Figure S6).

Next, we sought to investigate the relative orientation of hISG15 when bound to PLpro. As a starting point, we built a model of hISG15 bound to PLpro with MODELER[23] using the mouse complex (PDB entry 6YVA) as a template. In previous crystal structures of ISG15:PLpro complexes from MERS (PDB entry 6BI8), SARS-CoV (PDB entry 6YVA), and most recently SARS-CoV-2 (PDB entry 6XA9), the orientation of the C-terminal domain of ISG15 in the complex is conserved, interacting exclusively with the thumb and palm domains of PLpro (Figure S7). Therefore, we constrained the orientation of the C-terminal domain (spanning residues L82−G157) in complex with PLpro and used BILBOMD[24] to search for conformational states of the ISG15 N-terminal domain that would satisfy the SAXS data of the complex. PLpro, the C-terminal domain (L82−G157), and the N-terminal domain (M1−L73) of ISG15 were kept as rigid bodies, while the residues spanning the linker between the two ubiquitin domains (V74−P81) were allowed to be flexible in the simulation. The best fit to the SAXS (χ^2 = 1.15) was obtained from a mixture of three ISG15:PLpro conformers, indicating that the two domains are flexible and can move

https://doi.org/10.1021/acs.jpclett.1c00831
J. Phys. Chem. Lett. 2021, 12, 5608−5615

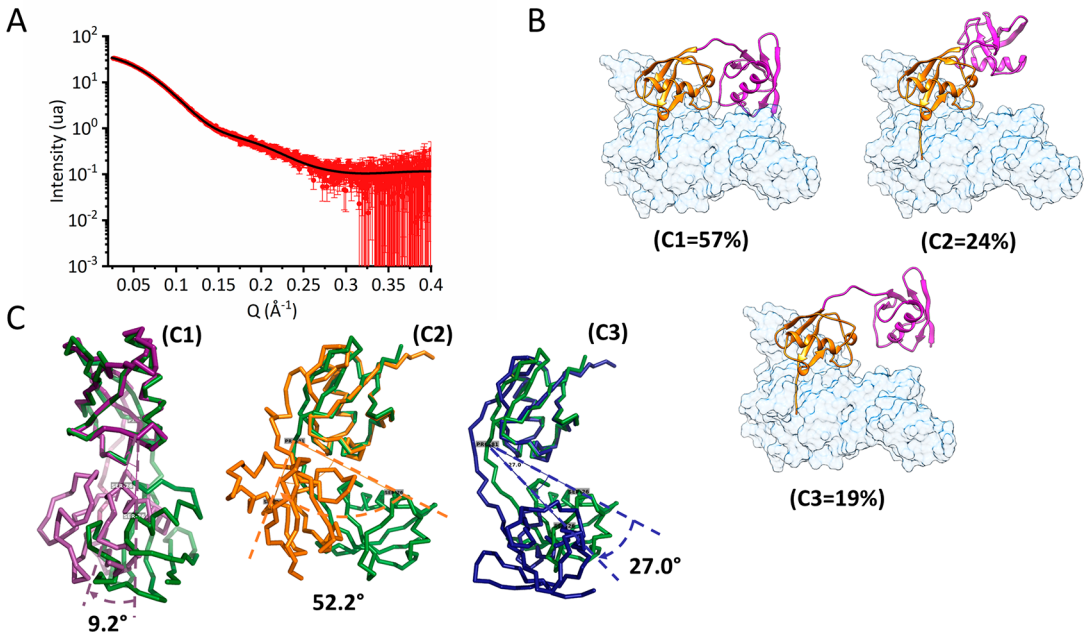

Figure 4. SEC-SAXS analysis of the PLpro C111S:hISG15 complex. (A) Comparison of the SAXS profile of the PLpro C111S:hISG15 complex and the theoretical SAXS curve for the ensemble of conformers in compact and extended conformations of the PLpro:ISG15 complex determined in the BILBOMD analysis, shown as red circles and a solid blue line, respectively. (B) Structural models of hISG15 conformers obtained from BILBOMD in complex with PLpro. The values represent the fraction that each conformer contributes to the overall fit to the SAXS of the PLpro:hISG15 complex shown in panel A. (C) Conformers C1 (purple), C2 (orange), and C3 (blue) were superposed with the ISG15 crystal structure (PDB entry 1Z2M, green). The twist angle of the N-terminal domain in each conformer was determined by the displacement of the Ser22 relative to Pro81, as it was presented by Langley et al.[20] The twist angle (82°) between C2 and free ISG15 was omitted for better visualization.

Table 2. Structural Distances of Free and Bound ISG15

	hISG15 alone (PDB entry 1Z2M)	mISG15 alone (PDB entry 5TLA)	mISG15 bound (PDB entry 6YVA)	conformer C1	conformer C2	conformer C3
UBL−UBL center of mass distance (Å)[a]	29.8	29.8	29.2	27.8	29.1	34.8
end-to-end distance (Å)[b]	45.5	50.3	43.7	45.0	58.3	57.4

[a]The centroid coordinates of the N- and C-terminal domains of ISG15 were defined using residues M1−V74 and L82−G157, respectively. The distance between the two centroids was defined as the distance of the center of mass of the two UBL domains using Chimera.[27] [b]The end-to-end distance was determined from the distance from M1 to G157 of hISG15, or the last residue present in each atomic structure.

relative to each other (Figure 4A). The three conformers, designated C1−C3, contribute 57%, 24%, and 19%, respectively, to the overall scattering profile (Table 2 and Figure 4B). A closer inspection of the ISG15 conformers that are overlaid using the residues comprising the C-terminal domain reveals that the N-terminal domains are twisted by 9.2°, 52.2°, and 27.0° in C1−C3, respectively, compared to the free protein, supporting the idea that hISG15 adopts a significantly different conformation when bound to PLpro. Interestingly, in the asymmetric unit of a USP18:mISG15 crystal structure, two different conformations for bound ISG15 were identified in which the N-terminal domains were located either 8 or 18 Å from the USP18 thumb domain, supporting conformational flexibility in ISG15 binding similar to what was observed in this study.[25] A recent study proposed that a conserved hydrophobic region present in the interdomain linker is important for interactions of ISG15s with binding partners. Residue variations in this region that are found in different species of ISG15s can lead to biochemical differences in ISG15−protein engagement.[6,20] Comparison of human, mouse, and bat ISG15s showed differences in how a conserved Phe40 is buried within the interface in the hydrophobic patch[20] that may explain the differences between PLpro:-mISG15 and PLpro:hISG15 complexes observed here. In addition, a conserved Pro39 present in most ISG15s is replaced by a histidine in the hISG15, which could result in steric and electrostatic factors that limit the conformations that ISG15 can adopt in different species.[6,26] These studies highlight the importance of the flexibility in the linker region in orienting the N-terminal domain of hISG15 in binding events, and also key N-terminal residues (Phe40 and His39) that play a role in the variability in the interdomain arrangement in all species.

The ISG15 conformers fit the contrast-matched PLpro-bound ISG15 SANS data well (χ^2 = 2.1 and 2.4, respectively), while the extended conformer yielded a relatively poor fit to the data, supporting the idea that a majority of the conformers are in the compact conformation when bound to PLpro (Figure 3C). Analysis of the binding interface of conformer C1 shows that the N-terminal domain of ISG15 shifted toward the thumb subdomain and is accommodated in a hydrophobic patch of PLpro (see a comparison in Figure S8A,B), and the compact ISG15 conformation is stabilized by electrostatic interactions (Figure S8C). The total binding interface area is 1295 Å^2. This area is ∼26% larger than the contact area formed between mISG15 and PLpro C111S (PDB entry 6YVA)

https://doi.org/10.1021/acs.jpclett.1c00831
J. Phys. Chem. Lett. 2021, 12, 5608−5615

(1026.5 Å^2). Contact residue pairs in the PLpro thumb subdomain and N-terminal domain of ISG15 with distances of <3 Å are E70 and S22, F69 and M23, T75 and E27, and Q174 and R54, respectively (Figure S8D).

In summary, using a combination of experimental and computational techniques, we have determined how the binding of PLpro from SARS-CoV-2 induces conformational changes in its substrate, hISG15. Although the flexible linker that connects the two ubiquitin-like domains in hISG15 suggests that the two domains can move freely and independently of each other, SAXS shows that the free ISG15 predominately exists in a preferentially extended state with the two ubiquitin domains spatially separated. Our analysis of the interaction of PLpro with hISG15 revealed two important details. First, the flexibility in the linker region is important in orienting the N-terminal domain in the complex. This is supported by a recent combined crystallography and isothermal calorimetry study of interactions of SARS-CoV-1 PLpro with ISG15s from different species that identified a hydrophobic interface between the two ubiquitin-like domains and revealed that ISG15 interdomain interactions play an important role in binding between ISG15 and other proteins.[20] Second, conformational plasticity exists in the interaction of the N-terminal domain when bound to PLpro that favors compact conformations of ISG15. This suggests that the N-terminal domain may weakly interact with PLpro compared to the C-terminal domain, which is known to bind tightly to PLpro in crystal structures. A recent nuclear magnetic resonance study also showed that the C-terminus of ISG15 dominates interactions with PLpro, supporting the analysis presented here.[13] In addition, an ovarian tumor (OTU) domain protease was shown to accommodate the C-terminal domain of ISG15 to facilitate its binding, supporting the idea that the C-terminal domain of ISG15 also dominates the interaction with other viral proteases.[28] This is in contrast to the interaction of PLpro with mouse ISG15, where it retains its extended conformation when bound to PLpro, and the orientation of the N-terminal ISG15 domain is rotated by almost 90° relative to the C-terminal domain (Figure S7).[8] This supports biochemical studies that show differences in the activity of PLpro with different species of ISG15 that on the basis of this work can be related to differences in binding interactions. This new knowledge is important for high-resolution structural studies of SARS-CoV-2 PLpro:ISG15 and approaches for drugs that target formation of this complex. Several potential noncovalent therapeutic agents have been developed to reduce the deISGylation activity of PLpro to impede viral replication.[13,29−32] The potency of these and future therapeutic compounds targeting the formation of the PLpro:hISG15 complex could be increased by utilizing our combination of X-ray crystallographic models, small-angle scattering, and computation that we used to develop a new model of the PLpro:hISG15 complex to optimize therapeutics to inhibit COVID-19 via inhibiting the formation of the PLpro:hISG15 complex.

■ ASSOCIATED CONTENT

Supporting Information

The Supporting Information is available free of charge at https://pubs.acs.org/doi/10.1021/acs.jpclett.1c00831.

Methods, protiated and deuterated protein expression and purification, SAXS and SANS experiments, SAXS and SANS data analysis and modeling, amino acid sequence and structure comparisons, figures, and references (PDF)

■ AUTHOR INFORMATION

Corresponding Authors

Leighton Coates − *Second Target Station, Oak Ridge National Laboratory, Oak Ridge, Tennessee 37831, United States;* orcid.org/0000-0003-2342-049X; Email: coatesl@ornl.gov

Hugh O'Neill − *Neutron Scattering Division, Oak Ridge National Laboratory, Oak Ridge, Tennessee 37831, United States;* orcid.org/0000-0003-2966-5527; Email: oneillhm@ornl.gov

Authors

Wellington C. Leite − *Neutron Scattering Division, Oak Ridge National Laboratory, Oak Ridge, Tennessee 37831, United States*

Kevin L. Weiss − *Neutron Scattering Division, Oak Ridge National Laboratory, Oak Ridge, Tennessee 37831, United States;* orcid.org/0000-0002-6486-8007

Gwyndalyn Phillips − *Neutron Scattering Division, Oak Ridge National Laboratory, Oak Ridge, Tennessee 37831, United States*

Qiu Zhang − *Neutron Scattering Division, Oak Ridge National Laboratory, Oak Ridge, Tennessee 37831, United States*

Shuo Qian − *Neutron Scattering Division, Oak Ridge National Laboratory, Oak Ridge, Tennessee 37831, United States;* orcid.org/0000-0002-4842-828X

Susan E. Tsutakawa − *Molecular Biophysics and Integrated Bioimaging, Lawrence Berkeley National Laboratory, Berkeley, California 94720, United States;* orcid.org/0000-0002-4918-4571

Complete contact information is available at: https://pubs.acs.org/10.1021/acs.jpclett.1c00831

Author Contributions

W.C.L. performed SANS and SAXS experiments, analyzed and interpreted the data, and performed the computational modeling. K.L.W., G.P., and Q.Z. expressed, purified, and characterized the proteins used in the study and produced isotopically labeled protein. S.Q. performed SANS experiments and interpreted the data. S.E.T. performed and analyzed SEC-SAXS experiments. L.C. conceived research, and L.C. and H.O'N led the study and wrote the manuscript with input from all co-authors.

Notes

The authors declare no competing financial interest.

■ ACKNOWLEDGMENTS

This research was supported by the U.S. Department of Energy (DOE) Office of Science through the National Virtual Biotechnology Laboratory (NVBL), a consortium of DOE National Laboratories focused on response to COVID-19, with funding provided by the Coronavirus CARES Act. Preliminary protein expression and purification studies were supported by the Laboratory Directed Research and Development Program at Oak Ridge National Laboratory (ORNL). The SARS-CoV-2 PLpro C111S expression plasmid (pMCSG53) was provided by Dr. Andrzej Joachimiak (Argonne National Laboratory,

Lemont, IL) with support from the National Institute of Allergy and Infectious Diseases, National Institutes of Health, Department of Health and Human Services, under Contract HHSN272201700060C. Bio-SANS is supported by ORNL's Center for Structural Molecular Biology funded by the DOE Office of Biological and Environmental Research. This research used resources at the High Flux Isotope Reactor and Spallation Neutron Source, a DOE Office of Science User Facility operated by the Oak Ridge National Laboratory. SAXS was conducted at the Advanced Light Source (ALS), a national user facility operated by Lawrence Berkeley National Laboratory on behalf of the DOE, Office of Basic Energy Sciences, through the Integrated Diffraction Analysis Technologies (IDAT) program, supported by DOE Office of Biological and Environmental Research. Additional support comes from National Institutes of Health Project ALS-ENABLE (P30 GM124169) and High-End Instrumentation Grant S10OD018483. L.C. acknowledges support from the Second Target Station, a DOE Office of Science User Facilities Construction Project at Oak Ridge National Laboratory. This manuscript has been authored by UT-Battelle, LLC, under Contract DE-AC05-00OR22725 with the DOE. The U.S. Government retains and the publisher, by accepting the article for publication, acknowledges that the U.S. Government retains a nonexclusive, paid-up, irrevocable, worldwide license to publish or reproduce the published form of this manuscript, or allow others to do so, for U.S. Government purposes. The DOE will provide public access to these results of federally sponsored research in accordance with the DOE Public Access Plan (http://energy.gov/downloads/doe-public-access-plan).

REFERENCES

(1) Wu, F.; Zhao, S.; Yu, B.; Chen, Y. M.; Wang, W.; Song, Z. G.; Hu, Y.; Tao, Z. W.; Tian, J. H.; Pei, Y. Y.; Yuan, M. L.; Zhang, Y. L.; Dai, F. H.; Liu, Y.; Wang, Q. M.; Zheng, J. J.; Xu, L.; Holmes, E. C.; Zhang, Y. Z. A new coronavirus associated with human respiratory disease in China. *Nature* **2020**, *579* (7798), 265−269.

(2) Kneller, D. W.; Phillips, G.; O'Neill, H. M.; Jedrzejczak, R.; Stols, L.; Langan, P.; Joachimiak, A.; Coates, L.; Kovalevsky, A. Structural plasticity of SARS-CoV-2 3CL M(pro) active site cavity revealed by room temperature X-ray crystallography. *Nat. Commun.* **2020**, *11* (1), 3202.

(3) Zhang, L.; Lin, D.; Sun, X.; Curth, U.; Drosten, C.; Sauerhering, L.; Becker, S.; Rox, K.; Hilgenfeld, R. Crystal structure of SARS-CoV-2 main protease provides a basis for design of improved alpha-ketoamide inhibitors. *Science* **2020**, *368*, 409.

(4) Lei, J.; Kusov, Y.; Hilgenfeld, R. Nsp3 of coronaviruses: Structures and functions of a large multi-domain protein. *Antiviral Res.* **2018**, *149*, 58−74.

(5) Ratia, K.; Saikatendu, K. S.; Santarsiero, B. D.; Barretto, N.; Baker, S. C.; Stevens, R. C.; Mesecar, A. D. Severe acute respiratory syndrome coronavirus papain-like protease: Structure of a viral deubiquitinating enzyme. *Proc. Natl. Acad. Sci. U. S. A.* **2006**, *103* (15), 5717−5722.

(6) Daczkowski, C. M.; Dzimianski, J. V.; Clasman, J. R.; Goodwin, O.; Mesecar, A. D.; Pegan, S. D. Structural Insights into the Interaction of Coronavirus Papain-Like Proteases and Interferon-Stimulated Gene Product 15 from Different Species. *J. Mol. Biol.* **2017**, *429* (11), 1661−1683.

(7) Dastur, A.; Beaudenon, S.; Kelley, M.; Krug, R. M.; Huibregtse, J. M. Herc5, an interferon-induced HECT E3 enzyme, is required for conjugation of ISG15 in human cells. *J. Biol. Chem.* **2006**, *281* (7), 4334−8.

(8) Shin, D.; Mukherjee, R.; Grewe, D.; Bojkova, D.; Baek, K.; Bhattacharya, A.; Schulz, L.; Widera, M.; Mehdipour, A. R.; Tascher, G.; Geurink, P. P.; Wilhelm, A.; van der Heden van Noort, G. J.; Ovaa, H.; Müller, S.; Knobeloch, K.-P.; Rajalingam, K.; Schulman, B. A.; Cinatl, J.; Hummer, G.; Ciesek, S.; Dikic, I. Papain-like protease regulates SARS-CoV-2 viral spread and innate immunity. *Nature* **2020**, *587*, 657.

(9) Freitas, B. T.; Durie, I. A.; Murray, J.; Longo, J. E.; Miller, H. C.; Crich, D.; Hogan, R. J.; Tripp, R. A.; Pegan, S. D. Characterization and Noncovalent Inhibition of the Deubiquitinase and deISGylase Activity of SARS-CoV-2 Papain-Like Protease. *ACS Infect. Dis.* **2020**, *6* (8), 2099−2109.

(10) Narasimhan, J.; Wang, M.; Fu, Z.; Klein, J. M.; Haas, A. L.; Kim, J. J. Crystal structure of the interferon-induced ubiquitin-like protein ISG15. *J. Biol. Chem.* **2005**, *280* (29), 27356−65.

(11) Klemm, T.; Ebert, G.; Calleja, D. J.; Allison, C. C.; Richardson, L. W.; Bernardini, J. P.; Lu, B. G.; Kuchel, N. W.; Grohmann, C.; Shibata, Y.; Gan, Z. Y.; Cooney, J. P.; Doerflinger, M.; Au, A. E.; Blackmore, T. R.; van der Heden van Noort, G. J.; Geurink, P. P.; Ovaa, H.; Newman, J.; Riboldi-Tunnicliffe, A.; Czabotar, P. E.; Mitchell, J. P.; Feltham, R.; Lechtenberg, B. C.; Lowes, K. N.; Dewson, G.; Pellegrini, M.; Lessene, G.; Komander, D. Mechanism and inhibition of the papain-like protease, PLpro, of SARS-CoV-2. *EMBO J.* **2020**, *39* (18), e106275.

(12) Rut, W.; Lv, Z.; Zmudzinski, M.; Patchett, S.; Nayak, D.; Snipas, S. J.; El Oualid, F.; Huang, T. T.; Bekes, M.; Drag, M.; Olsen, S. K. Activity profiling and crystal structures of inhibitor-bound SARS-CoV-2 papain-like protease: A framework for anti-COVID-19 drug design. *Sci. Adv.* **2020**, *6* (42), eabd4596.

(13) Fu, Z.; Huang, B.; Tang, J.; Liu, S.; Liu, M.; Ye, Y.; Liu, Z.; Xiong, Y.; Zhu, W.; Cao, D.; Li, J.; Niu, X.; Zhou, H.; Zhao, Y. J.; Zhang, G.; Huang, H. The complex structure of GRL0617 and SARS-CoV-2 PLpro reveals a hot spot for antiviral drug discovery. *Nat. Commun.* **2021**, *12* (1), 488.

(14) Huynh, T.; Cornell, W.; Luan, B. In silico Exploration of Inhibitors for SARS-CoV-2's Papain-Like Protease. *Front. Chem.* **2021**, *8*, 624163.

(15) Classen, S.; Hura, G. L.; Holton, J. M.; Rambo, R. P.; Rodic, I.; McGuire, P. J.; Dyer, K.; Hammel, M.; Meigs, G.; Frankel, K. A.; Tainer, J. A. Implementation and performance of SIBYLS: a dual endstation small-angle X-ray scattering and macromolecular crystallography beamline at the Advanced Light Source. *J. Appl. Crystallogr.* **2013**, *46* (Part 1), 1−13.

(16) Hura, G. L.; Menon, A. L.; Hammel, M.; Rambo, R. P.; Poole, F. L., 2nd; Tsutakawa, S. E.; Jenney, F. E., Jr.; Classen, S.; Frankel, K. A.; Hopkins, R. C.; Yang, S. J.; Scott, J. W.; Dillard, B. D.; Adams, M. W.; Tainer, J. A. Robust, high-throughput solution structural analyses by small angle X-ray scattering (SAXS). *Nat. Methods* **2009**, *6* (8), 606−12.

(17) Heller, W. T.; Urban, V. S.; Lynn, G. W.; Weiss, K. L.; O'Neill, H. M.; Pingali, S. V.; Qian, S.; Littrell, K. C.; Melnichenko, Y. B.; Buchanan, M. V.; Selby, D. L.; Wignall, G. D.; Butler, P. D.; Myles, D. A. The Bio-SANS instrument at the High Flux Isotope Reactor of Oak Ridge National Laboratory. *J. Appl. Crystallogr.* **2014**, *47* (4), 1238−1246.

(18) Heller, W. T. Small-angle neutron scattering and contrast variation: a powerful combination for studying biological structures. *Acta Crystallogr., Sect. D: Biol. Crystallogr.* **2010**, *66* (11), 1213−1217.

(19) Báez-Santos, Y. M.; St. John, S. E.; Mesecar, A. D. The SARS-coronavirus papain-like protease: structure, function and inhibition by designed antiviral compounds. *Antiviral Res.* **2015**, *115*, 21−38.

(20) Langley, C.; Goodwin, O.; Dzimianski, J. V.; Daczkowski, C. M.; Pegan, S. D. Structure of interferon-stimulated gene product 15 (ISG15) from the bat species Myotis davidii and the impact of interdomain ISG15 interactions on viral protein engagement. *Acta Crystallogr., Sect. D: Struct. Biol.* **2019**, *75* (Part 1), 21−31.

(21) Rambo, R. P.; Tainer, J. A. Characterizing flexible and intrinsically unstructured biological macromolecules by SAS using the Porod-Debye law. *Biopolymers* **2011**, *95* (8), 559−71.

(22) Akiyama, S.; Takahashi, S.; Kimura, T.; Ishimori, K.; Morishima, I.; Nishikawa, Y.; Fujisawa, T. Conformational landscape

https://doi.org/10.1021/acs.jpclett.1c00831
J. Phys. Chem. Lett. 2021, 12, 5608−5615

of cytochrome c folding studied by microsecond-resolved small-angle x-ray scattering. *Proc. Natl. Acad. Sci. U. S. A.* **2002**, *99* (3), 1329−34.
(23) Fiser, A.; Sali, A. Modeller: generation and refinement of homology-based protein structure models. *Methods Enzymol.* **2003**, *374*, 461−91.
(24) Pelikan, M.; Hura, G. L.; Hammel, M. Structure and flexibility within proteins as identified through small angle X-ray scattering. *Gen. Physiol. Biophys.* **2009**, *28* (2), 174−89.
(25) Basters, A.; Geurink, P. P.; Röcker, A.; Witting, K. F.; Tadayon, R.; Hess, S.; Semrau, M. S.; Storici, P.; Ovaa, H.; Knobeloch, K.-P.; Fritz, G. Structural basis of the specificity of USP18 toward ISG15. *Nat. Struct. Mol. Biol.* **2017**, *24* (3), 270−278.
(26) Dzimianski, J. V.; Scholte, F. E. M.; Bergeron, É.; Pegan, S. D. ISG15: It's Complicated. *J. Mol. Biol.* **2019**, *431* (21), 4203−4216.
(27) Pettersen, E. F.; Goddard, T. D.; Huang, C. C.; Couch, G. S.; Greenblatt, D. M.; Meng, E. C.; Ferrin, T. E. UCSF Chimera–a visualization system for exploratory research and analysis. *J. Comput. Chem.* **2004**, *25* (13), 1605−12.
(28) James, T. W.; Frias-Staheli, N.; Bacik, J.-P.; Levingston Macleod, J. M.; Khajehpour, M.; García-Sastre, A.; Mark, B. L. Structural basis for the removal of ubiquitin and interferon-stimulated gene 15 by a viral ovarian tumor domain-containing protease. *Proc. Natl. Acad. Sci. U. S. A.* **2011**, *108* (6), 2222−2227.
(29) Liu, C.; Zhou, Q.; Li, Y.; Garner, L. V.; Watkins, S. P.; Carter, L. J.; Smoot, J.; Gregg, A. C.; Daniels, A. D.; Jervey, S.; Albaiu, D. Research and Development on Therapeutic Agents and Vaccines for COVID-19 and Related Human Coronavirus Diseases. *ACS Cent. Sci.* **2020**, *6* (3), 315−331.
(30) Sheahan, T. P.; Sims, A. C.; Leist, S. R.; Schäfer, A.; Won, J.; Brown, A. J.; Montgomery, S. A.; Hogg, A.; Babusis, D.; Clarke, M. O.; Spahn, J. E.; Bauer, L.; Sellers, S.; Porter, D.; Feng, J. Y.; Cihlar, T.; Jordan, R.; Denison, M. R.; Baric, R. S. Comparative therapeutic efficacy of remdesivir and combination lopinavir, ritonavir, and interferon beta against MERS-CoV. *Nat. Commun.* **2020**, *11* (1), 222.
(31) Osipiuk, J.; Azizi, S.-A.; Dvorkin, S.; Endres, M.; Jedrzejczak, R.; Jones, K. A.; Kang, S.; Kathayat, R. S.; Kim, Y.; Lisnyak, V. G.; Maki, S. L.; Nicolaescu, V.; Taylor, C. A.; Tesar, C.; Zhang, Y.-A.; Zhou, Z.; Randall, G.; Michalska, K.; Snyder, S. A.; Dickinson, B. C.; Joachimiak, A. Structure of papain-like protease from SARS-CoV-2 and its complexes with non-covalent inhibitors. *Nat. Commun.* **2021**, *12* (1), 743.
(32) Maiti, B. K. Can Papain-like Protease Inhibitors Halt SARS-CoV-2 Replication? *ACS Pharmacology & Translational Science* **2020**, *3* (5), 1017−1019.

https://doi.org/10.1021/acs.jpclett.1c00831
J. Phys. Chem. Lett. 2021, 12, 5608−5615